Ultrasound-Induced Mechanical Compaction in Acoustically Responsive Scaffolds Promotes Spatiotemporally Modulated Signaling in Triple Negative Breast Cancer

Brock A. Humphries, Mitra Aliabouzar, Carole Quesada, Avinash Bevoor,
Kenneth K. Y. Ho, Alex Farfel, Johanna M. Buschhaus, Shrila Rajendran, Mario L. Fabiilli,*
and Gary D. Luker*

Cancer cells continually sense and respond to mechanical cues from the extracellular matrix (ECM). Interaction with the ECM can alter intracellular signaling cascades, leading to changes in processes that promote cancer cell growth, migration, and survival. The present study used a recently developed composite hydrogel composed of a fibrin matrix and phase-shift emulsion, termed an acoustically responsive scaffold (ARS), to investigate effects of local mechanical properties on breast cancer cell signaling. Treatment of ARSs with focused ultrasound drives acoustic droplet vaporization (ADV) in a spatiotemporally controlled manner, inducing local compaction and stiffening of the fibrin matrix adjacent to the matrix–bubble interface. Combining ARSs and live single cell imaging of triple-negative breast cancer cells, it is discovered that both basal and growth-factor stimulated activities of protein kinase B (also known as Akt) and extracellular signal-regulated kinase (ERK), two major kinases driving cancer progression, negatively correlate with increasing distance from the ADV-induced bubble both in vitro and in a mouse model. Together, these data demonstrate that local changes in ECM compaction regulate Akt and ERK signaling in breast cancer and support further applications of the novel ARS technology to analyze spatial and temporal effects of ECM mechanics on cell signaling and cancer biology.

1. Introduction

Rather than serving merely as an inert framework for tumors, research now clearly demonstrates that extracellular matrix (ECM) mechanics, architecture, and composition regulate key processes in tumor initiation, growth, and local invasion.[1–3] Increased deposition of ECM proteins in normal breast tissue, detected clinically as increased breast density on mammography, correlates with greater risk of breast cancer.[4] In breast cancer and multiple other malignancies, carcinoma-associated fibroblasts secrete and cross-link additional ECM proteins, elevating overall mechanical stiffness of a tumor relative to normal tissue. Stiffness and architecture evolve during tumor progression, adding time-dependent, varying inputs to cancer cells that may alter signaling and functions. While commonly considered as a macroscale property, breast tumors show regional and even microscale variations in ECM compaction with resultant effects on properties such as stiffness, porosity, and ligand density.[5–7] However, investigators largely have overlooked how local heterogeneities in ECM properties affect cancer cells. We propose that local differences in ECM properties elicit varying mechanosignaling and mechanobiologic effects on cancer cells, contributing to overall intercellular variations in behaviors of cancer cells.

B. A. Humphries, M. Aliabouzar, C. Quesada, A. Bevoor, K. K. Y. Ho,
A. Farfel, J. M. Buschhaus, S. Rajendran, M. L. Fabiilli, G. D. Luker
Department of Radiology
University of Michigan
Ann Arbor, MI 48109, USA
E-mail: mfabiill@umich.edu; gluker@umich.edu
B. A. Humphries, A. Bevoor, K. K. Y. Ho, A. Farfel, J. M. Buschhaus,
S. Rajendran, G. D. Luker
Center for Molecular Imaging
University of Michigan
Ann Arbor, MI 48109, USA

J. M. Buschhaus, M. L. Fabiilli, G. D. Luker
Department of Biomedical Engineering
University of Michigan
Ann Arbor, MI 48109, USA
M. L. Fabiilli
Applied Physics Program
University of Michigan
Ann Arbor, MI 48109, USA
G. D. Luker
Department of Microbiology and Immunology
University of Michigan
Ann Arbor, MI 48109, USA

**ADVANCED
SCIENCE NEWS**

www.advancedsciencenews.com

**ADVANCED
HEALTHCARE
MATERIALS**

www.advhealthmat.de

To advance our understanding of local, rather than macroscopic, effects of matrix compaction on cell signaling, we capitalized on our recent acoustically responsive scaffold (ARS) technology.[8] The ARS platform combines an ECM protein, such as fibrin, with perfluorocarbon (PFC)-containing phase-shift emulsions. Application of focused ultrasound, a noninvasive and clinically used technology, induces a liquid to gas phase transition of the emulsion, a mechanism known as acoustic droplet vaporization (ADV).[9,10] Focused ultrasound generates ADV at sub-millimeter resolution in an ARS, thereby creating a smart hydrogel platform with precise spatial and temporal control of micromechanical and microstructural changes in the ECM.[11–13] Specifically, our previous work demonstrated that the mechanical strain exerted on the surrounding matrix from ADV-generated bubbles resulted in significant, local compaction and stiffening of ECM adjacent to the matrix–bubble interface.[8] This radial compaction of the ECM is driven by the volumetric expansion of the PFC phase during ADV, which is approximately 125-fold, followed by growth of the ADV-generated gas bubble due to inward diffusion of gases in the local microenvironment (i.e., in-gassing). This ADV-induced stiffening occurs in strain stiffening matrices such as natural biopolymers like fibrin. Stiffening in fibrin-based ARSs, with initial Young's moduli of 0.2 kPa, ranged from ≈5-fold (1 h) to 20-fold (4 days) increases over nonbubble regions after ADV, which falls within the range of values measured in human breast tumors.[14–18] ADV-induced increases in stiffness within an ARS were hyperlocal[19] with significant differences observed at micron scale lengths and associated with concurrent decreases in matrix porosity. Our novel ARS technology allows us to create hydrogels with local, spatially defined, physiologically relevant variations in biophysical properties of the ECM. Because ECM properties like stiffness, porosity, and ligand density are interrelated, we refer to the ADV-induced changes to these properties in the ARS as ECM compaction.

Using ARSs, we investigated effects of temporally defined, local changes in ECM mechanical compaction on protein kinase B (also known as Akt) and extracellular signal-regulated kinase (ERK) signaling in triple-negative breast cancer (TNBC). Akt and ERK promote fundamental processes in tumor initiation and progression, including proliferation, survival, and invasion.[20,21] Activation of Akt and/or ERK occurs in ≈70% of TNBC, motivating efforts to understand ECM inputs controlling basal and growth-factor dependent regulation of these kinases. Using live, single-cell fluorescent imaging reporters to quantify Akt and ERK, we discovered that both basal and growth-factor stimulated activities of ERK and Akt in TNBC cells correlated negatively with distance from an ADV-induced bubble. We also used ARSs to control local mechanics and Akt and ERK activation in a mouse model, demonstrating the novel capability of this technology to readily transition from in vitro to in vivo settings. Overall, these data demonstrate the power of ARSs to modulate ECM compaction on a microscale level and reveal how local variations in ECM stiffness produce heterogeneity in cancer cell signaling.

2. Results

2.1. ADV Resulted in Local Fibrin Compaction and Stiffening in ARSs

Conversion of a phase-shift emulsion into a gas bubble via ADV resulted in consolidation of the fibrin matrix surrounding the bubble, thereby locally elevating the fluorescence signal within the matrix (**Figure 1**A). The time-dependent intensity profiles from the bubble–fibrin interface indicated that the diffusion-driven growth of the ADV-generated bubbles further increased the width of the consolidated fibrin region (Figure 1B,C). To assess the spatial variation in Young's moduli, we mapped moduli within approximately a 100 μm distance from the bubble–fibrin interface in an ARS (Figure 1D). The lowest and the highest measured Young's moduli within the interrogated distance were 0.18 and 3 kPa, respectively.

2.2. ADV-Induced Matrix Stiffening Enhances Kinase Activity in TNBC

We investigated how ADV-induced changes to the fibrin matrix affected signaling of TNBC cells encapsulated within the ARSs (**Figure 2**A). As fibrin is a physiologically relevant ECM component in breast tumors,[22,23] we used this system to capture effects of local matrix compaction on single-cell activation of Akt and ERK, kinases central to pathways mutated in over 30% of all cancers.[24] To study dynamics of Akt and ERK activities, we used MDA-MB-231 and SUM159 TNBC cells stably expressing fluorescent kinase translocation reporters (KTRs) for each kinase.[25] KTRs reversibly translocate between the cytoplasm and nucleus based upon phosphorylation of a known downstream substrate specific to Akt or ERK (Figure 2B). Accumulation of signal in the nucleus (dephosphorylated KTR) signifies that the kinase is "off," while signal in the cytoplasm (phosphorylated KTR) indicates that the kinase is "on." Although we define "off" and "on" states, we note that KTRs provide an analog readout of relative kinase activities. In addition to the Akt-KTR (fused to Aquamarine) and the ERK-KTR (fused to mCitrine), our reporter system also contains a histone H2B marker fused to mCherry to denote the nucleus. The nuclear marker allows simultaneous quantification of the KTR and distance of the cell from a bubble in the ARSs (Figure 2C).

To identify effects of ADV-induced matrix stiffening signaling on Akt and ERK activities, we used live-cell imaging to compare dynamics of the Akt and ERK KTRs in single cells in four different conditions: i) fibrin only gels, ii) fibrin gels with focused ultrasound, iii) ARSs, and iv) ARSs treated with ultrasound to generate ADV. In fibrin gels, Akt activity decreased in MDA-MB-231 cells over time in culture (**Figure 3**A; Figure S1, Supporting Information). Treatment of these gels with focused ultrasound did not significantly affect Akt activity (Table S1, Supporting Information). Consistent with these data, Akt activity decreased over time in ARSs without focused ultrasound. However, in striking contrast, treatment of ARSs with focused ultrasound
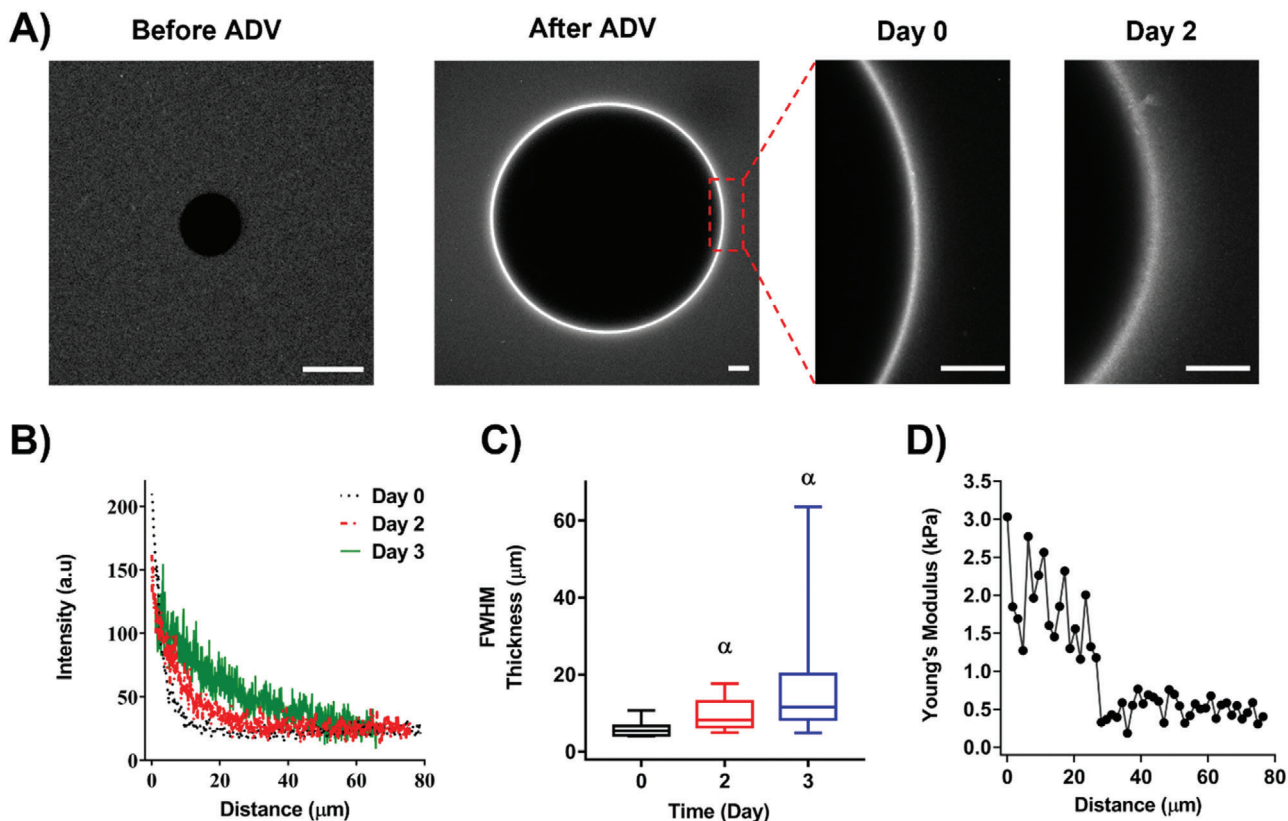
Figure 1. Acoustic droplet vaporization (ADV) resulted in local compaction and stiffening of fibrin surrounding the bubbles. A) Confocal microscopy images of acoustically responsive scaffolds (ARSs) before and after ADV are shown. For matrix visualization, ARSs contained Alexa Fluor 647-labeled fibrinogen (fibrinogen$_{647}$). B) Longitudinal, 1D intensity profiles of fibrinogen$_{647}$, were derived from confocal images containing a single ADV-generated bubble (like Day 0 and Day 2 images in panel A). 0 μm corresponds to the bubble–fibrin interface. C) Gaussian fitting was performed on the intensity profiles to calculate the full width at half-maximum (FWHM) thickness of the consolidated fibrin region ($n = 8$ (Day 0), $n = 13$ (Day 2), $n = 18$ (Day 3)). Statistically significant differences ($p < 0.05$) are denoted as follows: α versus Day 0. D) A 1D profile of the Young's modulus was generated 1 h post-ADV using atomic force microscopy. 0 μm corresponds to the bubble–fibrin interface. Scale bar: 20 μm.

enhanced Akt activity (Figure 3A; Figure S1, Supporting Information) to levels significantly higher than other combinations (Table S1, Supporting Information). Although MDA-MB-231 cells typically exhibit enhanced baseline activation of ERK due to mutant KRAS and BRAF,[26] we found that activity of ERK paralleled activity of Akt. ERK activity did not differ greatly among fibrin gels without the emulsion and ARSs without focused ultrasound. However, treatment of ARSs with focused ultrasound also significantly enhanced activity of ERK (Figure 3A; Figure S1 and Table S2, Supporting Information). SUM159 TNBC cells, which exhibit constitutively active Akt due to mutant phosphatidylinositol 3-kinase (PI3K),[26] also showed significantly enhanced activities of both Akt and ERK only in ARSs with focused ultrasound. (Figure S2A,B; Tables S3 and S4, Supporting Information). As a complementary method to investigate effects of hydrogel compaction on ERK and Akt activities in ARSs, we cultured cancer cells in gels with different densities of fibrin (2.5, 10, and 20 mg mL^{-1}) to progressively increase stiffness. Comparable to our ARSs, activities of ERK and Akt decreased over time in fibrin gels (Figures S3 and S4 and Tables S5–S8, Supporting Information) with increasing fibrin density generally maintaining greater signaling by these kinases. It is important to recognize that with fibrin hydrogels, matrix properties are interrelated. As such, an

increase in matrix density leads to simultaneous increases in matrix stiffness and ligand density as well as a decrease in matrix porosity.[27,28] Overall, these data, combined with our ARS experiments, demonstrate that the aforementioned matrix parameters contribute at least in part to enhanced kinase signaling.

2.3. Cells Proximal to the ADV-Induced Bubble Exhibit Increased Kinase Activities

We next investigated the relationship between Akt and ERK signaling and the distance of single cells from the ADV-induced bubble. Both Akt and ERK signaling decreased in MDA-MB-231 (Figure 3B) and SUM159 (Figure S5A, Supporting Information) cells with increasing distance from the ADV-induced bubble. Each day demonstrated a significantly nonzero linear regression for MDA-MB-231 cells ($p < 0.001$, 95% confidence intervals shown in Tables S9 and S10 in the Supporting Information). Consistent with these data, SUM159 cells also showed significantly nonzero linear regression (Day 1 ERK ($p < 0.01$), Day 2 Akt and ERK ($p < 0.001$), and Day 3 Akt and ERK graphs ($p < 0.01$), 95% confidence intervals shown in Tables S11 and S12 in the Supporting Information). Data from SUM159 cells show significantly
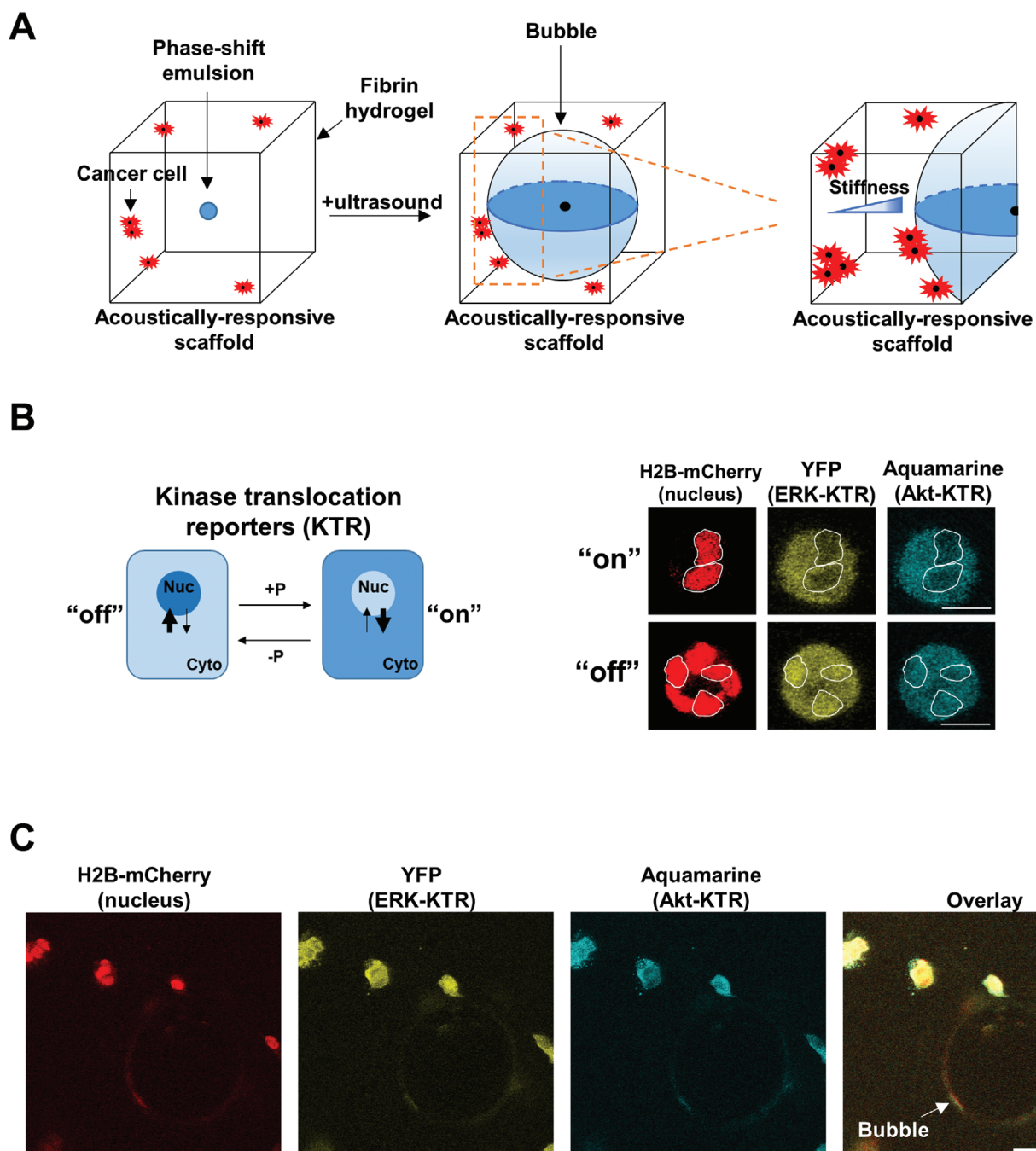
**ADVANCED
SCIENCE NEWS**

www.advancedsciencenews.com

**ADVANCED
HEALTHCARE
MATERIALS**

www.advhealthmat.de

Figure 2. Imaging acoustically responsive scaffolds containing breast cancer cells to measure cell signaling. A) Schematic of the acoustically responsive scaffold (ARS). ARSs containing breast cancer cells and a phase-shift emulsion (left) were exposed to focused ultrasound to generate acoustic droplet vaporization (ADV), which induces bubble formation and drives micromechanical and microstructural changes to the fibrin matrix (middle). These changes increase matrix compaction closer to a bubble (right). B) Schematic (left) and representative images (right) of ERK and Akt kinase translocation reporters (KTRs). Phosphorylation (+P) and dephosphorylation (−P) of the kinase substrate drives the reporter into the cytoplasm (kinase "on") or nucleus (kinase "off"), respectively. Scale bars are 20 µm. C) Representative images of MDA-MB-231 breast cancer cells containing kinase translocation reporters (KTRs) for both ERK and Akt kinases near a bubble (white arrow) generated by ADV. Scale bar is 50 µm.

enhanced Akt and ERK activity in the ARSs over time, contrasting with MDA-MB-231 cells under the same conditions. Dividing these cells into groups proximal (<100 µm) or distal (>100 µm) to a bubble demonstrated greater activities of Akt and ERK in cells proximal to the ADV-induced bubble in both MDA-MB-231

(Figure 3C) and SUM159 (Figure S5B, Supporting Information) cells. Activities of ERK and Akt decreased with time in ARSs, consistent with prior studies showing reduced signaling in 3D relative to 2D cultures.[29] We note that distributions of MDA-MB-231 cells relative to the bubble decrease with time, while we
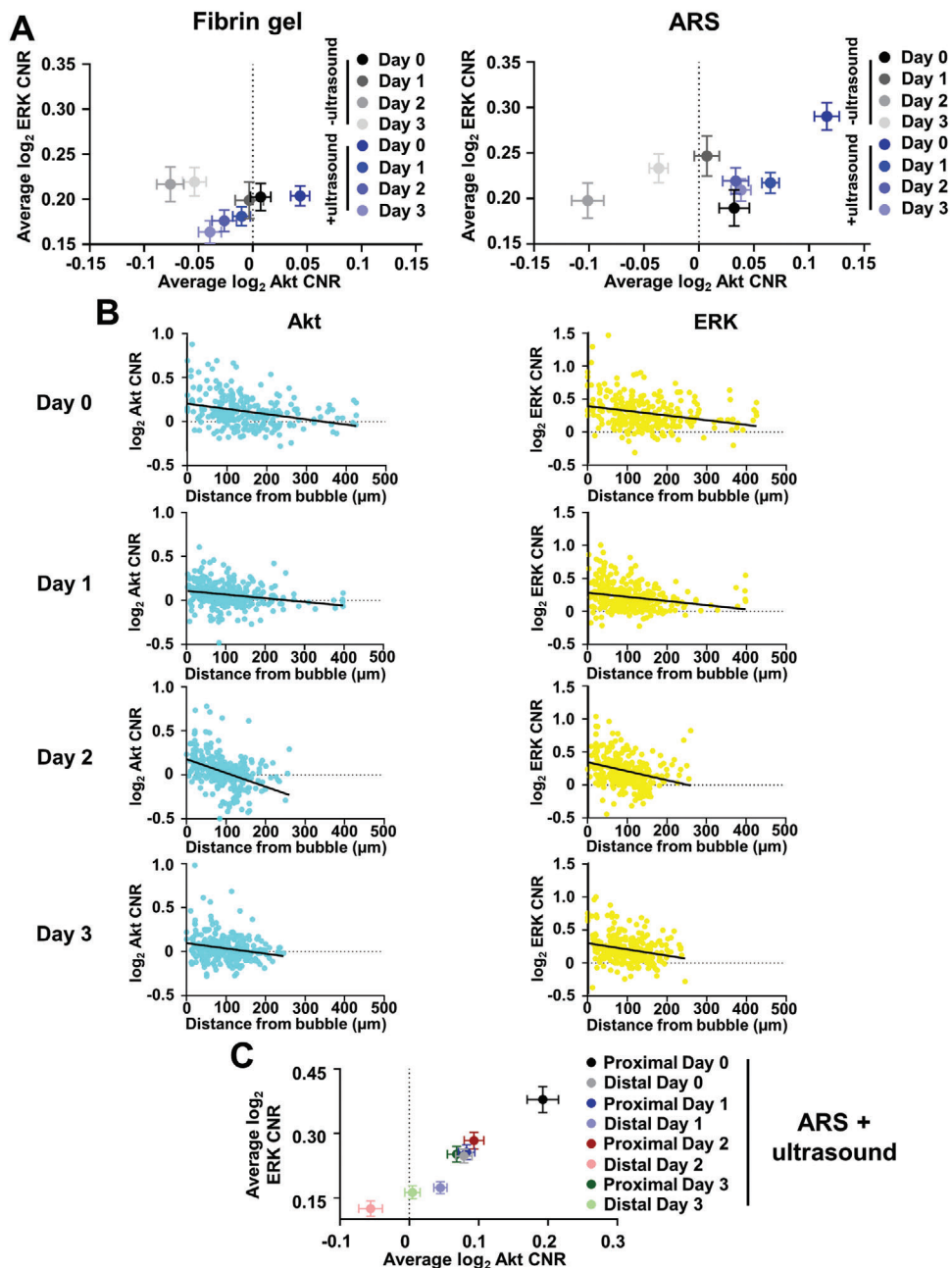
**ADVANCED
SCIENCE NEWS**

www.advancedsciencenews.com

**ADVANCED
HEALTHCARE
MATERIALS**

www.advhealthmat.de

Figure 3. Enhanced signaling in MDA-MB-231 breast cancer cells closer to the ADV-induced bubble. A) Graphs show mean ± SEM for Akt and ERK KTRs in MDA-MB-231 breast cancer cells treated with or without focused ultrasound cultured in ARSs without (left) or with (right) the phase-shift emulsion ($n \geq 117$ cells per group). We imaged cells immediately after focused ultrasound (Day 0) and for three subsequent days. B) We quantified activation of Akt (left) and ERK (right) ($n \geq 259$ cells per group) signaling relative to distance of the cell from the bubble surface, demonstrating that cells closest to the bubble surface signal more. All graphs show a significant nonzero linear regression ($p < 0.001$). C) Graph shows mean ± SEM $\log_2$ cytoplasmic-to-nuclear ratios (CNR) for Akt and ERK KTRs of cells close (<100 μm) or far (>100 μm) from the bubble at each time point ($n \geq 85$ cells per group). The CNR is the $\log_2$ measurement of the fluorescence intensity of the KTR in the cytoplasm relative to the fluorescence intensity of the KTR in the nucleus.

observed the opposite trend with SUM159 cells. We believe these differences arise from greater detection of SUM159 cells deeper in gels relative to MDA-MB-231 cells rather than inherent differences in biology. These data demonstrate that enhanced matrix compaction near an ADV-induced bubble drives increased activities of Akt and ERK relative to distal regions.

2.4. Cells Proximal to the ADV-Induced Bubble Show Increased Growth Factor Signaling

As data from Section 2.3 focus on baseline activities of ERK and Akt, we next investigated to what extent ADV-induced mechanical changes to the fibrin matrix altered immediate signaling

**ADVANCED
SCIENCE NEWS**

www.advancedsciencenews.com

**ADVANCED
HEALTHCARE
MATERIALS**

www.advhealthmat.de

responses to one-time stimulation with an established growth factor, epidermal growth factor (EGF). We cultured MDA-MB-231 cells in ARSs for three days after ADV; treated cells with EGF (50 ng mL^{-1}) as the stimulus and, using live-cell imaging; and quantified KTR activities for cells proximal (<100 µm) and distal (>100 µm) from the ADV-induced bubble. We observed heterogeneous Akt and ERK baseline activities, with single-cell responses to EGF ranging from strong (>0.5 log$_2$ CNR) to weak (<−0.5 log$_2$ CNR) activation of both Akt and ERK (**Figure 4**A). Although cells proximal to the bubble initially showed elevated activities of Akt and ERK, we still observed differences in cellular responses to ligand. Single-cell time tracks showed greater signaling responses to EGF in cells proximal to an ADV-induced bubble relative to those in distal regions (Figure 4B). Like data for baseline activities of Akt and ERK, responses to EGF correlated negatively with distance from an ADV-induced bubble. Cells located proximal to the ADV-induced bubble showed enhanced activity relative to those in distal regions (Figure 4C). Both Akt and ERK exhibited a significantly nonzero linear regression ($p < 0.01$, 95% confidence intervals shown in Table S13 in the Supporting Information). We also confirmed that ADV did not cause cytotoxicity to cells as defined by a LIVE/DEAD dye (Figure S6, Supporting Information), ruling out effects of cell death on signaling responses to EGF. Together, these results demonstrate that enhanced matrix compaction near an ADV-induced bubble corresponds to greater EGF-mediated signaling responses.

2.5. ARSs Drive Enhanced Akt and ERK Signaling In Vivo

To extend our data into an in vivo setting, we next injected ARSs containing MDA-MB-231 cells directly into the lower dorsal regions parallel to and on either side of the spine of nude mice. Two days after injection, we treated only one injection site with focused ultrasound. Immediately after injection, live-cell imaging showed heterogeneity in Akt and ERK activities between mice (**Figure 5**A). In one mouse, focused ultrasound produced modest increases in kinase activities, while the other mouse showed a marked increase in activities of Akt and ERK in the ARS treated with focused ultrasound. Quantification of Akt and ERK signaling three days after focused ultrasound produced more homogeneous data (Figure 5A). In each mouse, focused ultrasound increased Akt and ERK activities. Combining data from all mice (Figure 5B) showed significant increases in Akt and ERK activities in ARSs treated with focused ultrasound (Tables S14 and S15, Supporting Information). Furthermore, Akt and ERK activities in ARSs treated with focused ultrasound correlated with distance from an ADV-induced bubble (Figure 5C). Cells located proximal to an ADV-induced bubble showed enhanced activity relative to those in distal regions with both Akt and ERK having a significantly nonzero linear regression ($p < 0.001$, 95% confidence intervals shown in Table S16 in the Supporting Information). Together, these data demonstrate that mechanical compaction induced by ADV drives activation of Akt and ERK in mice.

3. Discussion

Developing more effective treatments for cancer requires better understanding of processes regulating key signaling pathways in tumor progression. Mechanical stiffening of ECM correlates with increased risk for breast cancer initiation and progression, but directly targeting ECM mechanics remains an unmet clinical challenge. While other studies demonstrate that enhanced ECM stiffness drives cell survival, proliferation, and motility,[30,31] mechanisms driving these fundamental processes in cancer remain poorly defined.

We investigated effects of local ECM compaction on single-cell activities of Akt and ERK, two major kinases driving essential steps in tumor initiation, progression, and metastasis in breast cancer and multiple other malignancies.[20,21] We leveraged an innovative ARS technology previously developed and characterized by our group. With this system, focused ultrasound generates ADV-induced bubbles in a fibrinogen/fibrin hydrogel containing a phase-shift emulsion. The technology provides several key biologic and biophysical advantages for this research. Fibrinogen/fibrin accumulates in the ECM of primary breast tumors and other malignancies,[22,32,33] making it a physiologically relevant matrix protein. Fibrin enhances survival of circulating tumor cells and promotes vascular extravasation in lung metastasis. Like other natural biopolymers, ADV-induced mechanical strain causes fibrin to exhibit strain stiffening,[8] increasing matrix density and reducing pore size in proximity to a bubble. Bubbles expand over time, creating progressively greater effects on local mechanical properties of the ARS. Focused ultrasound allows temporal control of bubble formation in the ARS. Temporal control allows us to directly compare kinase activities of breast cancer cells in hydrogels with the same composition. Focused ultrasound generates hydrogels with defined local variations in mechanical compaction rather than changing overall macroscopic mechanics and composition of the environment. Finally, our ARS technology produces well-characterized local variations in ECM compaction without detectable loss of viability of cells encapsulated in the hydrogel.

Other studies have identified effects of substrate stiffness on Akt and ERK activity.[34–36] We advance on these studies by combining our ARS technology with live, single-cell imaging to determine how activities of Akt and ERK respond to local differences in mechanics based on relative distances from ADV-induced bubbles. In 3D cell cultures and living mice, we discovered that local increases in ECM compaction increase basal and EGF-driven activities of Akt and ERK in two different triple-negative breast cancer cell lines. ECM compaction-dependent increases in both Akt and ERK occurred even in cells with constitutive activation of Akt due to a phosphatidyl-3-kinase mutation in SUM159 cells or ERK from KRas and BRaf mutations in MDA-MB-231 cells, respectively. Activities of Akt and ERK correlated positively with increases in ECM compaction as defined by distance from an ADV-induced bubble. Live-cell imaging with two-photon microscopy also revealed that ARSs activate Akt and ERK in breast cancer cells near ADV-induced bubbles when implanted into living mice. Effects of ADV-induced bubbles increased over time in vivo, likely because of progressive expansion of bubbles and associated local stiffness in ARSs. Collectively, these studies establish that local ECM compaction in a tumor environment, achieved without altering macroscopic composition of ECM, promotes Akt and ERK signaling in breast cancer.

Our research contributes to ongoing advances in technologies and approaches to understand how ECM stiffness drives
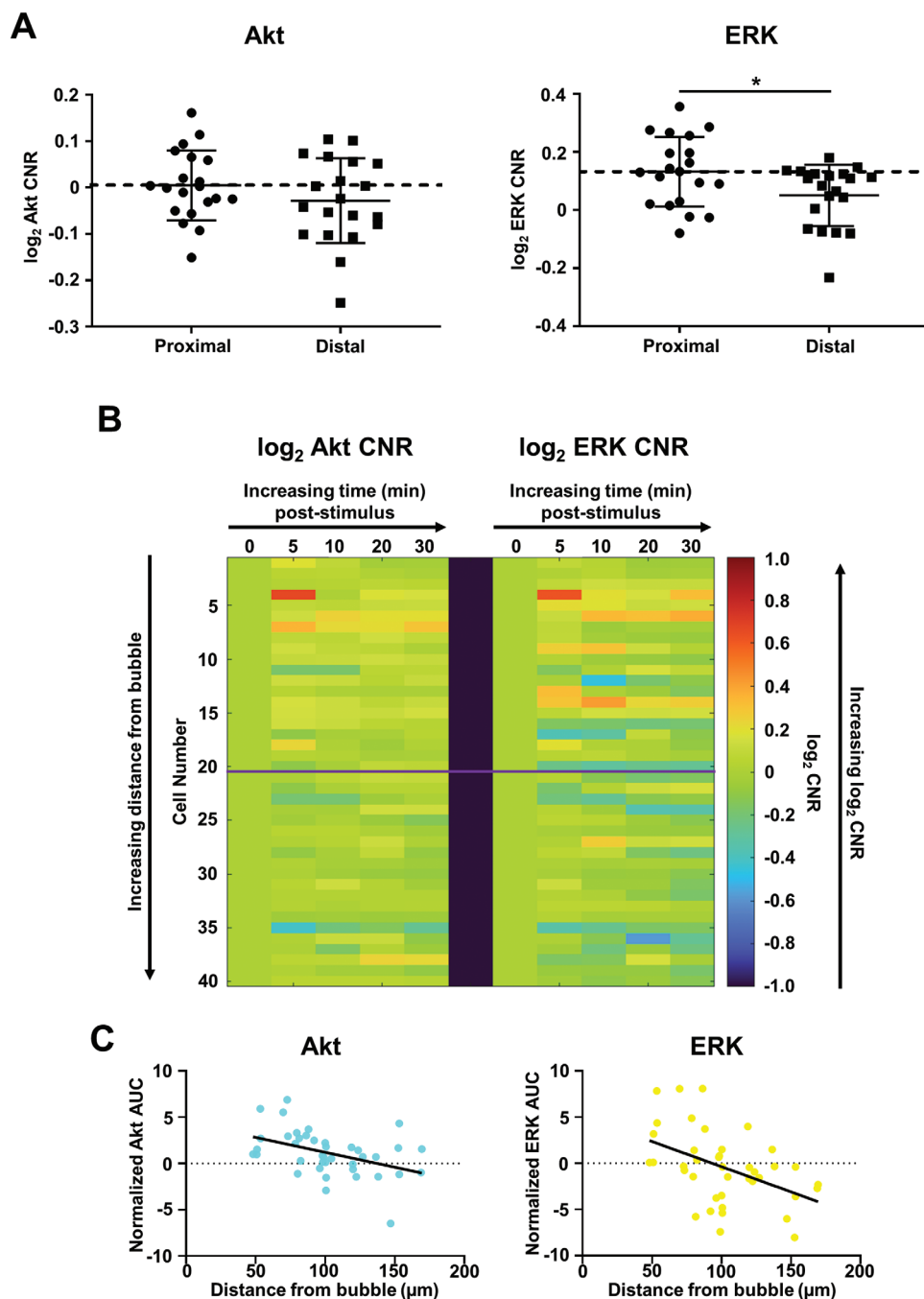
Figure 4. Cancer cells nearest the bubble surface show increased EGF signaling. After 3 days in an ARS, we performed time-lapse imaging of Akt and ERK KTRs before (0 min) and 30 min after addition of EGF (50 ng mL^{-1}). A) Graphs show summaries (mean ± SD) of Akt (left) and ERK (right) KTR activation at the initial time point before addition of EGF ($n = 20$ cells per group). $^{*}p < 0.05$. Dashed line represents the mean log$_2$ CNR in cells proximal (<100 μm) to the bubble. B) Single-cell time tracks show EGF-dependent activation of Akt and ERK in individual MDA-MB-231 breast cancer cells with KTR values displayed on a pseudocolor scale. We normalized data to Akt and ERK values at the initial time point for each cell (0 min). The graph sorts cells by distance from the bubble surface with cells nearest the bubble on top. The purple line separates cells nearest the bubble (<100 μm, $n = 20$ cells) from those furthest (>100 μm, $n = 20$ cells) from the bubble. C) Graphs show normalized area under the curve (AUC) for Akt (left) and ERK (right) signaling from (B) relative to distance of a cell from the bubble surface, demonstrating that cells most proximal to the bubble surface signal the most. Both graphs show a significant nonzero linear regression ($p < 0.01$).
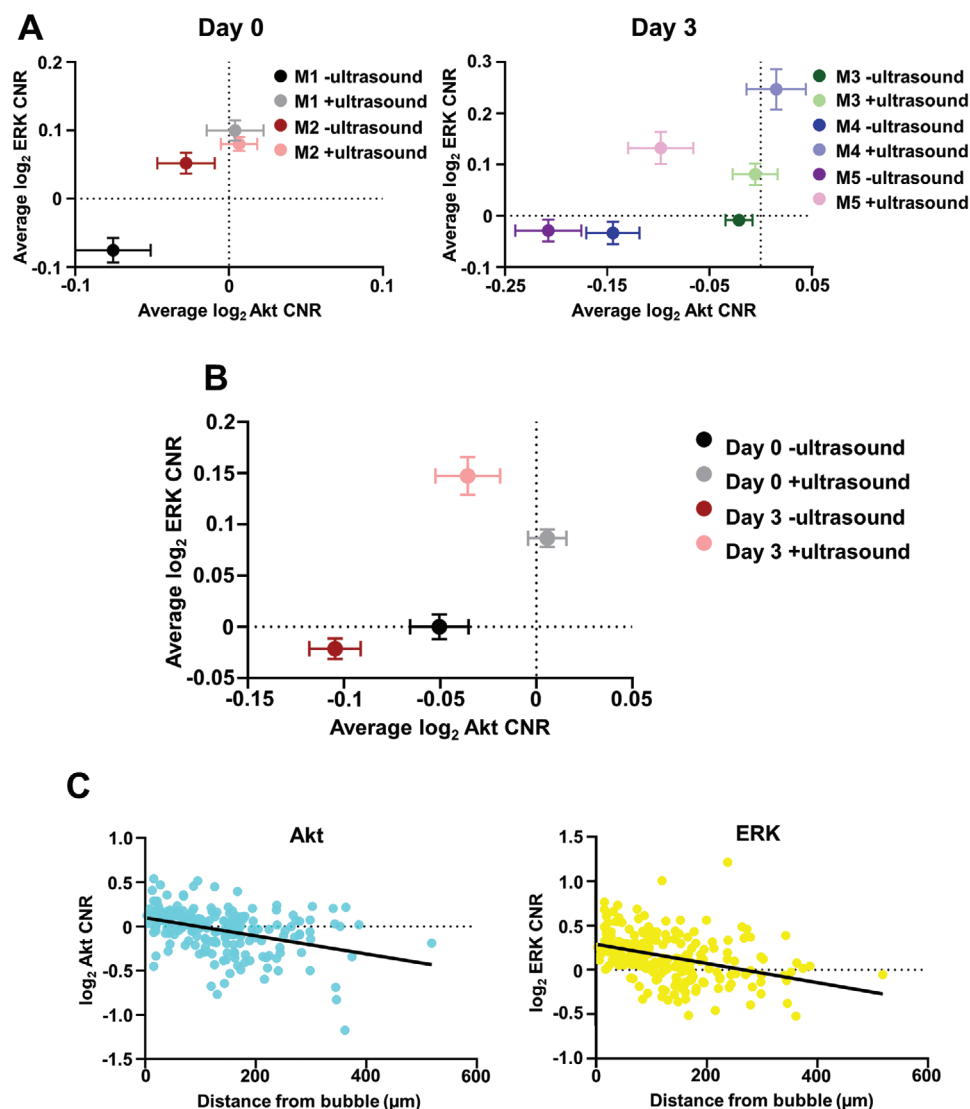
Figure 5. Acoustically responsive scaffolds (ARSs) increase MDA-MB-231 signaling in vivo. Graphs show mean ± SEM for Akt and ERK KTRs in MDA-MB-231 breast cancer cells treated with or without targeted ultrasound cultured in ARSs with the phase-shift double emulsion ($n \geq 60$ cells per group) in individual mice ($n = 2$ at Day 0 and $n = 3$ mice at Day 3) A) or with the mice combined B). We imaged cells immediately after targeted ultrasound (Day 0) and 3 days later (Day 3). C) We quantified and combined the activation of Akt (left) and ERK (right) ($n = 215$ cells per group) signaling relative to distance of a cell from the bubble surface for each mouse, demonstrating that cells closest to the bubble surface signal more. Both graphs show a significant nonzero linear regression ($p < 0.001$).

mechanotransduction in cancer. We and others have developed 3D hydrogel systems with tunable control of stiffness across the range present in normal breast tissue to advanced breast tumors.[37–40] These systems established that macroscopic ECM stiffness regulates multiple processes in cancer, including stem-like states, drug resistance, signaling, proliferation, invasion, and formation of blood vessels.[41,42] However, macroscopic measurements of overall stiffness of a hydrogel, particularly measurements done in the absence of cells, fail to detect local variations in stiffness caused by changes in distribution of ECM fibers, pore sizes, or matrix degradation by cells. Such variations contribute to heterogeneity of cellular behaviors observed among single cells embedded in hydrogels. Advances in material science have generated hydrogels with spatial and/or temporal control

of cross-linking or degradation to modify stiffness as a one-time change, gradients, or even reversibly.[43–45] The ability to dynamically change ECM conditions better recapitulates evolution of tumor environments.[46] Investigators use a variety of different stimuli to generate changes in ECM stiffness, including heat, ultraviolet light, and electric fields.[47–49] While effective at modulating ECM stiffness, heat, ultraviolet light and electric fields may damage cells embedded in hydrogels and/or not translate successfully to in vivo settings. Using focused ultrasound to dynamically control ECM compaction overcomes such limitations. As demonstrated previously and in this manuscript, our ARS technology produces local increases in ECM stiffness based on proximity to bubbles that progressively expand, producing time-dependent increases in mechanical force. Application of focused

**ADVANCED
SCIENCE NEWS**

www.advancedsciencenews.com

**ADVANCED
HEALTHCARE
MATERIALS**

www.advhealthmat.de

ultrasound caused no toxicity to cancer cells cultured in ARSs in vitro. We also showed that focused ultrasound with our ARS system successfully modulated kinase activities of breast cancer cells in hydrogels implanted into living mice. The ability to readily manipulate local ECM compaction in vivo opens new opportunities to investigate tumor mechanics in physiologic settings and potentially translate to applications in humans.

Cells sense mechanical changes in the ECM through a variety of cell surface molecules, including receptor tyrosine kinases, integrins, and G protein-coupled receptors. Exogenous force can cluster and activate these receptors, and expression of these receptors increases on cells cultured in more rigid environments.[50,51] As these families of receptors all signal through Akt and ERK, ECM compaction can activate these kinases through force-dependent regulation of cell surface receptors. Indeed, receptor levels and signaling are altered in stiff versus soft tumors, and these receptors can modify the tumorigenic behavior of a tissue.[52–54] Therefore, ECM compaction-mediated changes to cell surface receptors may explain enhanced basal and ligand-dependent activation of Akt and ERK in ARSs. Observed effects of mechanical compaction up to 100 μm on Akt and ERK are consistent other studies showing that breast cancer cells can sense mechanical signals a few hundred microns away.[55] In addition, time-dependent expansion of bubbles after focused ultrasound likely accounts for greater and more consistent increases in Akt and ERK between days 0 and 3 in hydrogels implanted into mice.

While ARSs with focused ultrasound generate defined gradients of mechanical compaction, we still observed heterogeneity in Akt and ERK activities at similar distances from a bubble. Intercellular variations in effects of compaction on these kinases indicate that other parameters, such as paracrine signaling, couple with compaction to control functions of cancer cells.[56] Single cells in seemingly uniform environments sense different amounts of force exerted on cell membranes, which also may contribute to heterogeneity in kinase activities in vitro and in vivo.[57] Future studies using single-cell imaging methods to measure membrane tension experienced by individual cells, in combination with KTRs, would allow us to directly relate local perceptions of compaction in each cell to kinase activities.[58] Such experiments would provide new insights into tumor heterogeneity and effects of ECM compaction on cell signaling and resultant effects on tumor initiation and progression in TNBC.

This study establishes ARSs as a stimulus-responsive, smart hydrogel technology to regulate local ECM compaction in a tumor environment. Coupling this system with live-cell imaging enables quantitative measurements of cell functions and behaviors, shifting studies of ECM mechanics from macroscopic, bulk measurements to single cells. As demonstrated in the current manuscript, our approach reveals heterogeneous responses of cancer cells to ECM compaction, producing intercellular differences in signaling through Akt and ERK. The ability to readily transition from in vitro systems to living animals provides a unique opportunity to investigate spatially and temporally controlled effects of ECM compaction on cancer biology and therapy. Future applications of the technology include investigations of durotaxis (migration in response to a stiffness gradient) with subsequent progression to metastasis, as well as both local effects of mechanical compaction and the combined biochemical

and mechanical cues of ADV on drug resistance and tumor recurrence. We also envision generating ARSs with other ECM proteins, allowing us to analyze how different combinations of ECM and compaction regulate behaviors of cancer cells. Future studies also will need to systematically quantify effects of each acoustic parameter on the induced compaction as well as map the micromechanical properties of the ARS to identify the scope of ADV-induced compaction. Additionally, elucidating relative contributions of ADV-induced changes to matrix properties like stiffness and ligand density, especially using synthetic hydrogels that enable decoupling of these properties, on cell behavior warrants further investigation.

4. Conclusion

In this study, we utilized ARSs to demonstrate that ADV-induced local stiffening of the fibrin matrix enhances Akt and ERK signaling in triple-negative breast cancer. Overall, we expect ARSs to advance research into mechanosignaling and mechanobiology, leading to novel approaches to improve cancer therapy by more effectively targeting ECM properties in tumors.

5. Experimental Section

Cell Culture: We purchased MDA-MB-231 cells from the ATCC (Manassas, VA, USA) and cultured these cells in Dulbecco's modified Eagle medium (DMEM) supplemented with 10% fetal bovine serum (FBS, Thermo Fisher Scientific, Waltham, MA, USA), 1% penicillin/streptomycin (Pen/Strep, Thermo Fisher Scientific, 15140148), and 1% GlutaMAX (Thermo Fisher Scientific, 35050061). We obtained SUM159 cells from Dr. Stephen Ethier (now at the Medical University of South Carolina, Charleston, SC, USA) and cultured these cells in F-12 media supplemented with 10% FBS, 1% Pen/Strep, 1% glutamine, 5 μg mL^{-1} hydrocortisone, and 1 μg mL^{-1} insulin. We authenticated all cells by analysis of short tandem repeats and characterized cells as free of *Mycoplasma* at the initial passage. We used all cells within 3 months after resuscitation and maintained all cells at 37 °C in a humidified incubator with 5% CO_2.

Preparation and Characterization of Monodisperse Phase Shift Emulsions: We prepared micrometer-sized emulsions with a double emulsion structure of water-in-PFC-in-water (W_1/PFC/W_2) using a microfluidic-based technique as described previously.[12] We used perfluoroheptane (C_7F_{16}, CAS# 335-57-9, bulk boiling point: 83 °C, Strem Chemicals, Newburyport, MA, USA) as the PFC phase. We combined the PFC solution at 2:1 (v/v) with a W_1 phase containing phosphate buffered saline (PBS, Life Technologies), and then sonicated (Q55 with CL-188 immersion probe, QSonica, LLC, Newton, CT, USA) for 30 s while on ice. We pumped the resulting primary emulsion and W_2 phase, comprised of 50 mg mL^{-1} Pluronic F68 (CAS# 9003-11-6, Sigma-Aldrich, St. Louis, MO, USA) in PBS, at 0.5 and 2.5 μL min^{-1}, respectively, through a quartz microfluidic chip (Cat# 3200146, junction: 14 μm × 17 μm, Dolomite, Royston, United Kingdom) to produce monodisperse phase-shift emulsion. We analyzed the average diameter, coefficient of variation, and concentration of the produced phase-shift emulsion using a Coulter Counter (Multisizer 4, Beckman Coulter, Brea, CA, USA) with a 50 μm aperture tube as 12.98 ± 0.8 μm, 3.3 ± 0.9%, and (3.5 ± 0.3) × 10^8 particles mL^{-1}, respectively.

Fabrication of Acoustically Responsive Scaffolds (ARSs): We prepared ARSs by first dissolving bovine fibrinogen (Sigma-Aldrich) in FluoroBrite Dulbecco's modified Eagle's medium (DMEM, Life Technologies) at 20 mg mL^{-1} clottable protein while under gentle vortex mixing for 30 s. We degassed the fibrinogen solution in a vacuum chamber (Isotemp vacuum oven, Model 282A, Fisher Scientific, Dubuque, IA, USA) to facilitate complete dissolution of the fibrinogen and minimize the amount of dissolved gas. For in vitro studies, ARSs (total volume: 0.3 mL; diameter: 15 mm; height: ≈1.7 mm) containing 10 mg mL^{-1} fibrin, 0.05 U mL^{-1} aprotinin,

**ADVANCED
SCIENCE NEWS**

www.advancedsciencenews.com

**ADVANCED
HEALTHCARE
MATERIALS**

www.advhealthmat.de

0.01% (v/v) phase-shift emulsion, 10^6 MDA-MB-231 cells mL^{-1}, and 2 U mL^{-1} thrombin were cast in 24-well BioFlex plates followed by polymerization for 15 min at room temperature. Acellular ARSs prepared for confocal microscopy analysis also contained 39 µg mL^{-1} Alexa Fluor 647-labeled fibrinogen (fibrinogen$_{647}$, F35200, Molecular Probes, Eugene, OR, USA). We coated each well in the BioFlex plate with 1% (w/v) solution of bovine serum albumin (Sigma-Aldrich) in PBS (for ≈30 min) prior to polymerization of the ARSs to facilitate removal of the scaffolds. Before ultrasound exposure, ARSs with complete FluoroBrite media (ThermoFisher Scientific, A1896701) containing 10% FBS, 1% Pen/Strep, 1% GlutaMAX, 1% sodium pyruvate (Thermo Fisher Scientific, Waltham, MA), and aprotinin (0.01 U mL^{-1}) were covered as described previously.[59]

Ultrasound Exposure Setup and Parameters: We exposed ARSs to ultrasound in a water tank (30 cm × 60 cm × 30 cm) filled with degassed (12–22% O_2 saturation), deionized water at 37 °C. We drove a calibrated, focused transducer (H147, f-number = 0.83, radius of curvature = 50 mm, Sonic Concepts Inc., Bothell, WA, USA) at its fundamental frequency (2.5 MHz) to generate acoustic droplet vaporization (ADV) within the ARSs. We generated pulsed waveforms (peak rarefactional pressure: 5 MPa, pulse duration: 5.4 µs; pulse repetition frequency: 100 Hz; duty cycle: 0.05%) by a function generator (33500B, Agilent Technologies, Santa Clara, CA, USA) and amplified by a gated radiofrequency amplifier (GA-2500A Ritec Inc., Warwick, RI, USA). This peak rarefactional pressure was previously shown to be suprathreshold for ADV within the ARSs containing C_7F_{16}– phase-shift emulsion.[60] We viewed and monitored the generated amplified signals in real time on an oscilloscope (HDO4034, Teledyne LeCroy, Chestnut Ridge, NY, USA).

We connected the transducer to a three-axis positioning system controlled by MATLAB (The MathWorks, Natick, MA, USA), localizing the transducer axially with respect to the ARSs using a pulse echo technique described previously.[13]

During ultrasound exposure, the transducer at a speed of 5 mm s^{-1} with a 0.5 mm lateral spacing between raster lines was rastered. Exposures were performed at three axial planes located 1.5, 1, and 0.5 mm above the well bottom with exposures completed from the top/distal (i.e., 1.5 mm) to bottom/proximal (i.e., 0.5 mm) direction.

Optical and Micromechanical Characterization of Acellular ARSs: To study the ADV-induced microstructural changes in the matrix, acellular ARSs were imaged over different time points with a laser scanning confocal microscope (LSM800, Zeiss, Pleasanton, CA, USA) using a 40× objective. The laser power was set to the lowest nonzero setting (0.2%) to minimize saturation. Intensity and full width half-maximum (FWHM) thickness measurements were performed on selected confocal images using ZEN lite software (Zeiss).

Atomic force microscopy was performed on ARSs using the TT-AFM (AFM Workshop, CA, USA). ARSs were mechanically interrogated using a precalibrated probe (nominal spring constant: 0.064 N m^{-1}, Novascan, IA, USA) with a spherical glass bead (radius: 1 µm). The compressive Young's modulus was approximated from the force–indentation curves using AtomicJ software (http://sourceforge.net/projects/jrobust) as described previously.[8]

Kinase Translocation Reporter (KTR) Signaling in Fibrin Gels and ARSs: To quantify activation of both ERK and Akt kinases in single cells, we used previously validated KTRs.[25] KTRs measure activities of ERK and Akt by utilizing a known downstream substrate specific for each kinase fused to a fluorescent protein.[61,62] This KTR construct contains histone 2B (H2B) fused to mCherry (H2B-mCherry), the Akt-KTR reporter (Aquamarine), the ERK-KTR reporter (mCitrine), and a puromycin selection marker all separated by P2A linker sequences cloned into the Piggybac transposon vector as described previously (pHAEP).[25,59,63] We cotransfected the pHAEP vector and the Piggybac transposase into breast cancer cells and selected for stable integrants with puromycin.[25] We verified expression of the full pHAEP reporter construct by fluorescence microscopy.

To determine effects of enhanced mechanical compaction near the ADV-induced bubble on Akt and ERK signaling, we formed ARSs containing MDA-MB-231- or SUM159-pHAEP cells containing click beetle green (CBG) luciferase initially cultured on 2D plastic at a final concentration of 1×10^6 cells mL^{-1}. We covered ARSs with complete FluoroBrite me-

dia containing the additives mentioned above. Two days after fabrication of the ARSs, we treated them with focused ultrasound and imaged immediately after (Day 0) and each subsequent day for 3 days (Days 1–3) using an Olympus FVMPE-RS upright two-photon microscope with settings as described previously.[25] We changed media daily. We determined activation of Akt and ERK in the ARSs by quantifying the cytoplasmic-to-nuclear ratio (CNR) of fluorescence intensities in individual cells as described previously.[25] We measured the distance of individual cells from the surface of the ADV-induced bubble.

To further investigate effects of hydrogel mechanics on Akt and ERK signaling in the absence of ultrasound, we embedded single cells (1×10^6 mL^{-1}) in gels with increasing densities of fibrin (i.e., 2.5, 10, or 20 mg mL^{-1} fibrin) to increase stiffness. Gels also contained 2 U mL^{-1} thrombin, 0.05 U mL^{-1} aprotinin, and no phase-shift emulsion as described previously.[64]

To determine effects of the ADV-driven increase in mechanical compaction on signaling response to ligand, we formed ARSs containing MDA-MB-231-CBG-pHAEP and cultured them for three days after focused ultrasound as described above. We then treated cells with 50 ng mL^{-1} epidermal growth factor (EGF, R&D Systems, Minneapolis, MN, USA) and acquired images at the times listed in the figure. At the end of the time course, we incubated ARSs with a LIVE/DEAD stain (ThermoFisher Scientific, L34966) and imaged to determine viability of cells.

Mouse Studies: The University of Michigan Institutional Animal Care and Use Committee approved all animal procedures (protocol 00008822). The animals used in this study received humane care in compliance with the principles of laboratory animal care formulated by the National Society for Medical Research and Guide for the Care and Use of Laboratory Animals prepared by the National Academy of Sciences and published by the National Institute of Health (Publication no NIH 85-23, revised 1996).

We implanted ARSs (final concentrations: fibrinogen (10 mg mL^{-1}), aprotinin (0.05 U mL^{-1}), thrombin (2 U mL^{-1}), emulsion (0.01% v/v), and 1×10^6 MDA-MB-231-CBG-pHAEP cells mL^{-1}) in vivo by orthotopic injection into the lower dorsal region parallel to and on either side of the spine of 6-7-week-old male *Foxn1^{nu}* mice (Charles River, Wilmington, MA, USA, $n = 5$) as described previously.[65] Two days after injection, we treated one dorsal side of each mouse with focused ultrasound and imaged both dorsal injections immediately (Day 0, $n = 2$ mice) or three days later (Day 3, $n = 3$ mice). We quantified the KTRs of cells in ARSs in vivo by two-photon microscopy using the excitation and emission filters described above.

Statistical Analysis: For experiments comparing only two groups, we used two-tailed, unpaired student's t-tests. For experiments comparing multiple groups, we used one-way ANOVA and Tukey's multiple comparisons test. For Akt and ERK signaling relative to the distance from the ADV-induced bubble, we used linear regression analysis. We considered a significance level of $p < 0.05$ statistically significant. We prepared column graphs (mean values + SD as denoted in figure legend), X–Y plots (mean values + SEM as denoted in figure legends), and box plots and whiskers using GraphPad Prism 8. For box plots and whiskers, the bottom and top of a box define the first and third quartiles, and the band inside the box marks the second quartile (the median). The ends of the whiskers represent the 10th and 90th percentiles, respectively. For all box plots and whiskers, the "+" within the box refers to the mean.

Supporting Information

Supporting Information is available from the Wiley Online Library or from the author.

Acknowledgements

**ADVANCED
SCIENCE NEWS**

www.advancedsciencenews.com

**ADVANCED
HEALTHCARE
MATERIALS**

www.advhealthmat.de

Conflict of Interest

G.D.L. serves as a consultant and receives research funding from Polyphor, Ltd., which is now part of Spexis. All other authors declare no competing interests.

Author Contributions

M.L.F and G.D.L. are senior coauthors. B.A.H., M.A., M.L.F., and G.D.L. participated in research design. B.A.H., M.A., C.Q., A.B., K.K.Y.H., A.F., S.R., and J.M.B. conducted experiments. B.A.H., M.A., and K.K.Y.H. performed the data analysis. B.A.H., M.A., M.L.F., and G.D.L. wrote the manuscript. All authors contributed to editing the article and approved the submitted version.

Data Availability Statement

The data that support the findings of this study are available from the corresponding author upon reasonable request.

Keywords

[1] P. Lu, K. Takai, V. M. Weaver, Z. Werb, *Cold Spring Harb. Perspect. Biol.* **2011**, *3*, a005058.

[2] J. D. Humphrey, E. R. Dufresne, M. A. Schwartz, *Nat. Rev. Mol. Cell Biol.* **2014**, *15*, 802.

[3] F. Spill, D. S. Reynolds, R. D. Kamm, M. H. Zaman, *Curr. Opin. Biotechnol.* **2016**, *40*, 41.

[4] C. Byrne, C. Schairer, J. Wolfe, N. Parekh, M. Salane, L. A. Brinton, R. Hoover, R. Haile, *J. Natl. Cancer Inst.* **1995**, *87*, 1622.

[5] P. Lu, V. M. Weaver, Z. Werb, *J. Cell Biol.* **2012**, *196*, 395.

[6] B. M. Baker, B. Trappmann, W. Y. Wang, M. S. Sakar, I. L. Kim, V. B. Shenoy, J. A. Burdick, C. S. Chen, *Nat. Mater.* **2015**, *14*, 1262.

[7] A. J. Berger, K. M. Linsmeier, P. K. Kreeger, K. S. Masters, *Biomaterials* **2017**, *141*, 125.

[8] M. Aliabouzar, C. D. Davidson, W. Y. Wang, O. D. Kripfgans, R. T. Franceschi, A. J. Putnam, J. B. Fowlkes, B. M. Baker, M. L. Fabiilli, *Soft Matter* **2020**, *16*, 6501.

[9] O. D. Kripfgans, J. B. Fowlkes, D. L. Miller, O. P. Eldevik, P. L. Carson, *Ultrasound Med. Biol.* **2000**, *26*, 1177.

[10] P. S. Sheeran, S. H. Luois, L. B. Mullin, T. O. Matsunaga, P. A. Dayton, *Biomaterials* **2012**, *33*, 3262.

[11] M. L. Fabiilli, C. G. Wilson, F. Padilla, F. M. Martin-Saavedra, J. B. Fowlkes, R. T. Franceschi, *Acta Biomater.* **2013**, *9*, 7399.

[12] A. Moncion, M. Lin, E. G. O'Neill, R. T. Franceschi, O. D. Kripfgans, A. J. Putnam, M. L. Fabiilli, *Biomaterials* **2017**, *140*, 26.

[13] M. Aliabouzar, A. Jivani, X. Lu, O. D. Kripfgans, J. B. Fowlkes, M. L. Fabiilli, *Ultrason. Sonochem.* **2020**, *66*, 105109.

[14] L. Kass, J. T. Erler, M. Dembo, V. M. Weaver, *Int. J. Biochem. Cell Biol.* **2007**, *39*, 1987.

[15] D. T. Butcher, T. Alliston, V. M. Weaver, *Nat. Rev. Cancer* **2009**, *9*, 108.

[16] K. Lee, Q. K. Chen, C. Lui, M. A. Cichon, D. C. Radisky, C. M. Nelson, *Mol. Biol. Cell* **2012**, *23*, 4097.

[17] M. Plodinec, M. Loparic, C. A. Monnier, E. C. Obermann, R. Zanetti-Dallenbach, P. Oertle, J. T. Hyotyla, U. Aebi, M. Bentires-Alj, R. Y. Lim, C. A. Schoenenberger, *Nat. Nanotechnol.* **2012**, *7*, 757.

[18] M. F. Pang, M. J. Siedlik, S. Han, M. Stallings-Mann, D. C. Radisky, C. M. Nelson, *Cancer Res.* **2016**, *76*, 5277.

[19] E. Farrell, M. Aliabouzar, C. Quesada, B. M. Baker, R. T. Franceschi, A. J. Putnam, M. L. Fabiilli, *Acta Biomater.* **2021**, *138*, 133.

[20] J. A. McCubrey, L. S. Steelman, W. H. Chappell, S. L. Abrams, E. W. Wong, F. Chang, B. Lehmann, D. M. Terrian, M. Milella, A. Tafuri, F. Stivala, M. Libra, J. Basecke, C. Evangelisti, A. M. Martelli, R. A. Franklin, *Biochim. Biophys. Acta* **2007**, *1773*, 1263.

[21] B. D. Manning, A. Toker, *Cell* **2017**, *169*, 381.

[22] V. Constantini, L. R. Zacharski, V. A. Memoli, W. Kisiel, B. J. Kudryk, S. M. Rousseau, *Cancer Res.* **1991**, *51*, 349.

[23] P. J. Simpson-Haidaris, B. Rybarczyk, *Ann. N. Y. Acad. Sci.* **2001**, *936*, 406.

[24] N. Cancer Genome Atlas Research, J. N. Weinstein, E. A. Collisson, G. B. Mills, K. R. Shaw, B. A. Ozenberger, K. Ellrott, I. Shmulevich, C. Sander, J. M. Stuart, *Nat. Genet.* **2013**, *45*, 1113.

[25] P. C. Spinosa, B. A. Humphries, D. Lewin Mejia, J. M. Buschhaus, J. J. Linderman, G. D. Luker, K. E. Luker, *Sci. Signal.* **2019**, *12*, eaaw4204.

[26] A. Hollestelle, F. Elstrodt, J. H. Nagel, W. W. Kallemeijn, M. Schutte, *Mol. Cancer Res.* **2007**, *5*, 195.

[27] C. M. Ghajar, K. S. Blevins, C. C. W. Hughes, S. C. George, A. J. Putnam, *Tissue Eng.* **2006**, *12*, 2875.

[28] H. Duong, B. Wu, B. Tawil, *Tissue Eng., Part A* **2009**, *15*, 1865.

[29] N. Abe-Fukasawa, R. Watanabe, Y. Gen, T. Nishino, N. Itasaki, *FEBS J.* **2021**, *288*, 5650.

[30] M. J. Bissell, W. C. Hines, *Nat. Med.* **2011**, *17*, 320.

[31] D. F. Quail, J. A. Joyce, *Nat. Med.* **2013**, *19*, 1423.

[32] H. F. Dvorak, D. R. Senger, A. M. Dvorak, *Cancer Metastasis Rev.* **1983**, *2*, 41.

[33] V. Constantini, L. R. Zacharski, *Cancer Metastasis Rev.* **1992**, *11*, 283.

[34] C. Liu, X. Li, J. Feng, F. Liao, D. Li, D. Han, *Clin. Hemorheol. Microcirc.* **2016**, *63*, 399.

[35] R. Zhang, M. Ma, G. Dong, R. R. Yao, J. H. Li, Q. D. Zheng, Y. Y. Dong, H. Ma, D. M. Gao, J. F. Cui, Z. G. Ren, R. X. Chen, *Cancer Sci.* **2017**, *108*, 1778.

[36] M. Sun, G. Chi, J. Xu, Y. Tan, J. Xu, S. Lv, Z. Xu, Y. Xia, L. Li, Y. Li, *Stem Cell Res. Ther.* **2018**, *9*, 52.

[37] C. Liu, D. Lewin Mejia, B. Chiang, K. E. Luker, G. D. Luker, *Acta Biomater.* **2018**, *75*, 213.

[38] H. M. Micek, M. R. Visetsouk, K. S. Masters, P. K. Kreeger, *iScience* **2020**, *23*, 101742.

[39] J. Vasudevan, C. T. Lim, J. G. Fernandez, *Adv. Funct. Mater.* **2020**, *30*, 2005383.

[40] C. Liu, M. Li, Z. X. Dong, D. Jiang, X. Li, S. Lin, D. Chen, X. Zou, X. D. Zhang, G. D. Luker, *Acta Biomater.* **2021**, *131*, 326.

[41] M. R. Zanotelli, C. A. Reinhart-King, *Adv. Exp. Med. Biol.* **2018**, *1092*, 91.

[42] Y. Li, R. Randriantsilefisoa, J. Chen, J. L. Cuellar-Camacho, W. Liang, W. Li, *ACS Appl. Bio Mater.* **2020**, *3*, 4474.

[43] R. Yang, H. Liang, *RSC Adv.* **2018**, *8*, 6675.

[44] M. G. Ondeck, A. Kumar, J. K. Placone, C. M. Plunkett, B. F. Matte, K. C. Wong, L. Fattet, J. Yang, A. J. Engler, *Proc. Natl. Acad. Sci. USA* **2019**, *116*, 3502.

[45] E. Hopkins, E. Valois, A. Stull, K. Le, A. A. Pitenis, M. Z. Wilson, *ACS Biomater. Sci. Eng.* **2021**, *7*, 408.

[46] J. Winkler, A. Abisoye-Ogunniyan, K. J. Metcalf, Z. Werb, *Nat. Commun.* **2020**, *11*, 5120.

[47] J. A. Burdick, C. Chung, X. Jia, M. A. Randolph, R. Langer, *Biomacromolecules* **2005**, *6*, 386.

[48] M. Guvendiren, J. A. Burdick, *Nat. Commun.* **2012**, *3*, 792.

[49] R. S. Stowers, S. C. Allen, L. J. Suggs, *Proc. Natl. Acad. Sci. USA* **2015**, *112*, 1953.

[50] M. Delcommenne, C. H. Streuli, *J. Biol. Chem.* **1995**, *270*, 26794.

[51] M. J. Paszek, N. Zahir, K. R. Johnson, J. N. Lakins, G. I. Rozenberg, A. Gefen, C. A. Reinhart-King, S. S. Margulies, M. Dembo, D. Boettiger, D. A. Hammer, V. M. Weaver, *Cancer Cell* **2005**, *8*, 241.

[52] W. Guo, F. G. Giancotti, *Nat. Rev. Mol. Cell Biol.* **2004**, *5*, 816.

[53] D. E. White, N. A. Kurpios, D. Zuo, J. A. Hassel, S. Blaess, U. Mueller, W. J. Muller, *Cancer Cell* **2004**, *6*, 159.

[54] V. Mieulet, C. Garnier, Y. Kieffer, T. Guilbert, F. Nemati, E. Marangoni, G. Renault, F. Chamming's, A. Vincent-Salomon, F. Mechta-Grigoriou, *Sci. Rep.* **2021**, *11*, 4219.

[55] Q. Shi, R. P. Ghosh, H. Engelke, C. H. Rycroft, L. Cassereau, J. A. Sethian, V. M. Weaver, J. T. Liphardt, *Proc. Natl. Acad. Sci. USA* **2014**, *111*, 658.

[56] L. Yang, P. Shi, G. Zhao, J. Xu, W. Peng, J. Zhang, G. Zhang, X. Wang, Z. Dong, F. Chen, H. Cui, *Signal Transduct. Target. Ther.* **2020**, *5*, 8.

[57] C. Grashoff, B. D. Hoffman, M. D. Brenner, R. Zhou, M. Parsons, M. T. Yang, M. A. McLean, S. G. Sligar, C. S. Chen, T. Ha, M. A. Schwartz, *Nature* **2010**, *466*, 263.

[58] A. S. LaCroix, A. D. Lynch, M. E. Berginski, B. D. Hoffman, *Elife* **2018**, *7*, e33927.

[59] B. A. Humphries, A. C. Cutter, J. M. Buschhaus, Y. C. Chen, T. Qyli, D. S. W. Palagama, S. Eckley, T. H. Robison, A. Bevoor, B. Chiang, H. R. Haley, S. Sahoo, P. C. Spinosa, D. B. Neale, J. Boppisetti, D. Sahoo, P. Ghosh, J. Lahann, B. D. Ross, E. Yoon, K. E. Luker, G. D. Luker, *Breast Cancer Res.* **2020**, *22*, 60.

[60] X. Lu, X. Dong, S. Natla, O. D. Kripfgans, J. B. Fowlkes, X. Wang, R. Franceschi, A. J. Putnam, M. L. Fabiilli, *Ultrasound Med. Biol.* **2019**, *45*, 2471.

[61] S. Regot, J. J. Hughey, B. T. Bajar, S. Carrasco, M. W. Covert, *Cell* **2014**, *157*, 1724.

[62] G. Maryu, M. Matsuda, K. Aoki, *Cell Struct. Funct.* **2016**, *41*, 81.

[63] B. A. Humphries, J. M. Buschhaus, Y. C. Chen, H. R. Haley, T. Qyli, B. Chiang, N. Shen, S. Rajendran, A. Cutter, Y. H. Cheng, Y. T. Chen, J. Cong, P. C. Spinosa, E. Yoon, K. E. Luker, G. D. Luker, *Mol. Cancer Res.* **2019**, *17*, 1142.

[64] H. Zhao, L. Ma, J. Zhou, Z. Mao, C. Gao, J. Shen, *Biomed. Mater.* **2008**, *3*, 015001.

[65] X. Lu, H. Jin, C. Quesada, E. C. Farrell, L. Huang, M. Aliabouzar, O. D. Kripfgans, J. B. Fowlkes, R. T. Franceschi, A. J. Putnam, M. L. Fabiilli, *Acta Biomater.* **2020**, *113*, 217.